

Numerical Calculation of Radiation from A Long Antenna Situated On A Photonic Crystal Substrate

J. Merle Elson

Naval Air Warfare Center Weapons Division
Research Department, Signals and Sensors Division
China Lake, CA 93555

Mark Fahey

Computer Sciences Corporation
Engineer Research and Development Center MSRC
Vicksburg, MS 39180-6199

Abstract

Properties of electronic components are intimately related to quantum physics associated with the behavior of electrons in a periodic crystalline structure environment. Similarly, photons propagating in a periodic structure can exhibit behavior analogous to an electron propagating in an electronic crystal. Obviously, electronic components/devices are ubiquitous and have vastly changed our way of life. It follows that research into properties and applications of photonic crystalline devices could lead to equally widespread use and value to all facets of society.

Typically, there can be one or more gaps in the range of allowable energy an electron propagating in a semiconductor crystal can have. In the sense of how an electronic device functions, such forbidden energy band gaps can be fundamental. Analogous band gaps can occur for the allowable energies of photons propagating in a periodic dielectric structure, i.e., photonic crystal (PC). It is this physical property that we wish to exploit in this work.

The theory portion of this work involves using perfectly matched layer (PML) boundary conditions, the R-matrix propagator algorithm, and a finite-difference frequency-domain modal-expansion approach to calculate antenna radiation. The antenna is mounted adjacent to a finite-sized PC substrate and is driven at frequencies below, within, and above the band gap associated with an infinite PC. The PC and antenna are invariant along one dimension. The PC consists of a two-dimensional finite-sized square array of dielectric rods with square cross section.

Numerical examples of radiation patterns are given for various frequencies. Typical numerical tasks include linear equation solution, matrix multiplication, and calculating eigenvalues and eigenvectors. Most of the computational effort involves repetitious calculation of

eigenvalues and eigenvectors. To reduce wallclock time, a complex parallel eigensolver was developed.

Introduction

We model the photonic crystal (PC) and antenna structure as shown in Fig. 1. The basic objective of this work is to solve Maxwell's equations throughout the PC. The physical size of the PC is L_x and L_z in the x and z direction, respectively, and within these finite dimensions, the PC is periodic with period a . The PC is an array of square-cross-section dielectric rods with permittivity ϵ_r embedded in a background medium with permittivity ϵ_b . The top layer of the PC from $z = L_z$ to $z = L_z + h$ is the antenna layer with permittivity ϵ_b except for the antenna, which has permittivity ϵ_a . The vertical regions, which are shaded gray near the left and right x limits of the PC, indicate the Berenger Perfectly Matched Layer (PML) [1] absorbing regions which facilitate numerical calculation by preventing unwanted reflection from the edges of the computational domain. The PML regions are designed to simulate an infinite spatial domain by absorbing (with negligible reflection) any wave that reaches the edge of the calculation domain.

The L_x and L_z dimensions of the PC are typically many wavelengths in length and because of the periodic nature of the PC, we know that possible solutions will generally consist of evanescent as well as propagating waves. The R-matrix propagator method [2-4] is proven to be numerically stable and well suited for problems having computational domain sizes which can be many wavelengths in dimension. In addition, many computational techniques are limited to structures where infinite periodicity is used to reduce the computational size of the problem. This restriction must be eliminated for devices and problems where periodicity is non-existent. In this paper we present an implementation of Berenger's PML[1] formalism for the R-matrix method to eliminate this restriction. Also, we present results of a parallel complex eigensolver for non-symmetric matrices.

Theory

Referring to Fig. 1, note the numerous horizontal dashed lines separating regions of the PC. These lines indicate regions that are by definition z invariant and in this work, such regions will be called layers henceforth. We will describe in this section how we find solutions to Maxwell's equations within a layer and then connect all layer solutions together. The problem analyzed here is two-dimensional, and the PC structure consists of a truncated square array of dielectric rods. The rectangular cross section antenna lies atop the PC and the antenna current is assumed to have only a y component and to be uniform throughout the antenna cross section. There are a finite number of rows of rods and each row has a finite number of rods in each row. The example in Fig. 1 shows five rows with nine rods in each row. Each row of rods has a homogeneous spacer layer in between. The superstrate $z \geq L_z + h$ and substrate $z \leq 0$ regions are homogeneous and assumed to be vacuum.

Maxwell's equations and PML absorbing layers

In the context of a finite-difference-time-domain approach to solve Maxwell's equations, Berenger [1] incorporated impedance-matched absorbing boundary layers. The present work is done in the frequency domain, but we also want to incorporate the absorbing layers in the vicinity of the x limits of the PC region. We assume $\exp(-i\omega t)$ time dependence. The PML absorbing layers are characterized by anisotropy in the electric σ and magnetic σ^* conductivity. For the case here where the PC and antenna current are y invariant, only transverse electric (TE) polarization is appropriate and the following discussion will assume TE polarization. In the time domain, the essence of a PML absorbing medium is to split the electric field into two parts: $E_y = E_{yx} + E_{yz}$ and further distinguish between conductivity relating to absorption along the x ($\mathbf{s}_x, \mathbf{s}_x^*$) and z ($\mathbf{s}_z, \mathbf{s}_z^*$) directions. However in this two-dimensional work and in the frequency domain, field splitting is not required. After some manipulation and combining equations, the analogous equations to Berenger's[1] work can be shown to be equivalent to

$$\frac{\partial E_y(x, z)}{\partial z} = -\frac{i\omega}{c} \mathbf{m}_z(x, z) B_x(x, z) \quad (1)$$

$$\frac{\partial B_x(x, z)}{\partial z} = -\frac{i\omega}{c} \mathbf{e}_z(x, z) E_y(x, z) + \frac{\mathbf{e}_z(x, z)}{\mathbf{e}_x(x, z)} \frac{\partial}{\partial x} \left[\frac{c}{i\omega \mathbf{m}_x(x, z)} \frac{\partial E_y(x, z)}{\partial x} \right] + \frac{4\mathbf{p}}{c} J_y(x, z) \quad (2)$$

where $J_y(x, z)$ is the antenna current and for brevity we define

$$\mathbf{e}_x(x, z) = \mathbf{e}(x, z) + 4\mathbf{p}\mathbf{s}_x(x, z)/\omega, \quad \mathbf{m}_x(x, z) = 1 + 4\mathbf{p}\mathbf{s}_x^*(x, z)/\omega, \quad (3)$$

$$\mathbf{e}_z(x, z) = \mathbf{e}(x, z) + 4\mathbf{p}\mathbf{s}_z(x, z)/\omega, \quad \text{and} \quad \mathbf{m}_z(x, z) = 1 + 4\mathbf{p}\mathbf{s}_z^*(x, z)/\omega. \quad (4)$$

Note that we write the antenna current as a function of x and z , but we assume the current is zero everywhere outside the antenna cross section but uniform within the cross section. Outside of any PML region, the $\mathbf{s}_x = \mathbf{s}_x^* = \mathbf{s}_z = \mathbf{s}_z^* = 0$, and Eqs. (1)-(4) reduce to the usual form of Maxwell's equations. In Eqs. (3) and (4), we also make the simplifying assumption that the material parameters (permittivity and PML conductivity) in certain regions are independent of coordinate z . As pointed out earlier, z invariance applies to any PC region between adjacent dashed lines shown in Fig. 1. We further note that there is no need to create a PML region that has absorption for propagation in the z direction. This means that we set $\mathbf{s}_z = \mathbf{s}_z^* = 0$ everywhere. After applying these simplifications to Eqs. (1)-(4), we then combine these two equations into a second order differential equation as

$$\frac{\partial^2 E_y(x, z)}{\partial z^2} = -\frac{i\omega}{c} \frac{4\mathbf{p}}{c} J_y(x) - \left(\frac{\omega}{c}\right)^2 \mathbf{e}(x) E_y(x, z) - \frac{\mathbf{e}(x)}{\mathbf{e}_x(x)} \frac{\partial}{\partial x} \left[\frac{1}{\mathbf{m}_x(x)} \frac{\partial E_y(x, z)}{\partial x} \right]. \quad (5)$$

The finite-difference part of this work comes from discretizing the x dimension into N segments where $x = n\Delta x$ and $\Delta x = L/N$. We approximate the x derivatives in Eq. (5) in centered finite-difference form. This yields

$$\begin{aligned} \frac{\partial^2 E_y(n\Delta x, z)}{\partial z^2} = & -\frac{i\mathbf{w}}{c} \frac{4\mathbf{p}}{c} J_y(n\Delta x) - \left(\frac{\mathbf{w}}{c}\right)^2 \mathbf{e}(n\Delta x) E_y(n\Delta x, z) \\ & - \frac{\mathbf{e}(n\Delta x)}{\Delta x^2 \mathbf{e}_x(n\Delta x)} \left\{ \frac{E_y((n+1)\Delta x, z) - E_y(n\Delta x, z)}{\mathbf{m}_x((n+1/2)\Delta x)} + \frac{E_y((n-1)\Delta x, z) - E_y(n\Delta x, z)}{\mathbf{m}_x((n-1/2)\Delta x)} \right\}. \end{aligned} \quad (6)$$

In Eq. (6), the \mathbf{s}_x and \mathbf{s}_x^* are zero everywhere except in a PML region and impedance matching requires that we set $\mathbf{s}_x/\mathbf{e} = \mathbf{s}_x^*$.

The x coordinate is now a discrete variable, but the z coordinate remains a continuous variable. Equation (6) is valid in a layer of the PC where $\mathbf{e}(x)$, $\mathbf{e}_x(x)$ and $\mathbf{m}(x)$ are by definition independent of z for all x . Since Eq. (6) is valid at N discrete points x , we have N coupled differential equations for each z -invariant layer. All N differential equations for a given layer as in Eq. (6) may be concisely written in matrix form as

$$\frac{\partial^2 E(z)}{\partial z^2} = \mathbf{M}E(z) - 4i\mathbf{p}\mathbf{w}J/c^2. \quad (7)$$

Explicit x dependence notation and y component notation from Eq. (6) has been omitted and is understood in Eq. (7) where \mathbf{M} is a $N \times N$ square matrix. The electric field $E(z)$ and source term J are N -element column vectors where each element corresponds to a discrete coordinate x . The source term is zero everywhere except in the antenna region of the topmost layer. Since \mathbf{M} and J are independent of z , the solution for the fields in a layer is straightforward by diagonalization of \mathbf{M} as $\mathbf{S}^{-1}\mathbf{M}\mathbf{S} = \mathbf{1}^2 = \mathbf{1} \cdot \mathbf{1}$, and this yields the modal solutions

$$E(z) = \mathbf{S}(\exp(\mathbf{I}z)\mathbf{C}_+ + \exp(-\mathbf{I}z)\mathbf{C}_-) + \frac{4i\mathbf{p}\mathbf{w}}{c^2} \mathbf{M}^{-1}J \quad (8)$$

$$B(z) = \left(\frac{ic}{\mathbf{w}}\right) \mathbf{S} \mathbf{1} (\exp(\mathbf{I}z)\mathbf{C}_+ - \exp(-\mathbf{I}z)\mathbf{C}_-) . \quad (9)$$

The $N \times N$ square matrix \mathbf{S} in Eqs. (8) and (9) has columns that are the eigenvectors of \mathbf{M} and the associated N eigenvalues are the elements of the diagonal matrix $\mathbf{1}^2$. Clearly, we must compute N eigenvalues and eigenvectors for each layer of the PC. The $\exp(\pm \mathbf{I}z)$ are $N \times N$ diagonal matrices with the non-zero elements being exponential terms and \mathbf{C}_\pm are column vectors of constants. The arguments of the diagonal terms in the $\exp(\pm \mathbf{I}z)$ matrices contain N pairs $\pm \mathbf{I}$ that are the $2N$ roots of the diagonal terms of the matrix $\mathbf{1}^2$. The solutions E and B , are the y and x components of the electric and magnetic fields, respectively, and these fields are continuous across layer boundaries.

R-Matrix algorithm

We discuss matrices in this section denoted by \mathbf{r}_{ij} and \mathbf{R}_{ij} ($i = 1, 2$ and $j = 1, 2$). These matrices, which are instrumental to the R-matrix algorithm, provide field relationships between the boundaries of a layer and across two or more layers, respectively. This algorithm is numerically stable for computational sizes which are many wavelengths in dimension and which contain evanescent terms.

R-Matrix without sources

Equations (8) and (9) yield solutions within a layer and in the following, we describe how these solutions are related between multiple layers. For those layers which have no source currents (i.e., $J = 0$ in Eqs. (7) and (8)), the R-matrix algorithm involves calculating a matrix relationship between the electric and magnetic fields at the boundaries of a z invariant layer of thickness Δz . This relationship has the form

$$\begin{pmatrix} E(z) \\ E(z + \Delta z) \end{pmatrix} = \begin{pmatrix} \mathbf{r}_{11}(\Delta z) & \mathbf{r}_{12}(\Delta z) \\ \mathbf{r}_{21}(\Delta z) & \mathbf{r}_{22}(\Delta z) \end{pmatrix} \begin{pmatrix} B(z) \\ B(z + \Delta z) \end{pmatrix}. \quad (10)$$

As shown in Fig.1, since all the layers between $z = 0$ to $z = L_z$ are source free, Eq. (10) can be applied to each of these layers and the $N \times N$ \mathbf{r}_{ij} submatrices relate the electric and magnetic fields at the two boundaries of a single layer. For each layer in the PC, the \mathbf{r}_{ij} matrices can be calculated by using Eq. (8) (with $J = 0$) and Eq. (9) in Eq. (10) and this yields

$$\mathbf{r}_{11}(\Delta z) = \left(\frac{i\omega}{c} \right) \mathbf{S} (\exp(I\Delta z) + \exp(-I\Delta z)) (\exp(I\Delta z) - \exp(-I\Delta z))^{-1} \mathbf{l}^{-1} \mathbf{S}^{-1} \mathbf{m} \quad (11)$$

$$\mathbf{r}_{12}(\Delta z) = \left(\frac{-2i\omega}{c} \right) \mathbf{S} (\exp(I\Delta z) - \exp(-I\Delta z))^{-1} \mathbf{l}^{-1} \mathbf{S}^{-1} \mathbf{m} \quad (12)$$

and $\mathbf{r}_{22}(\Delta z) = -\mathbf{r}_{11}(\Delta z)$ and $\mathbf{r}_{21}(\Delta z) = -\mathbf{r}_{12}(\Delta z)$. The $N \times N$ square matrix \mathbf{m} is a diagonal matrix with non-zero elements obtained from Eq. (3). While Eqs. (10)-(12) relate fields across a single layer, we also need a global relationship of the form

$$\begin{pmatrix} E(z=0) \\ E(z=L) \end{pmatrix} = \begin{pmatrix} \mathbf{R}_{11}(L) & \mathbf{R}_{12}(L) \\ \mathbf{R}_{21}(L) & \mathbf{R}_{22}(L) \end{pmatrix} \begin{pmatrix} B(z=0) \\ B(z=L) \end{pmatrix} \quad (13)$$

that can span many layers. Similar to the \mathbf{r}_{ij} matrices, the \mathbf{R}_{ij} submatrices relate fields at boundaries $z = 0$ and $z = L$ which enclose all z -invariant layers. By sequentially calculating the \mathbf{r}_{ij} matrices for each layer in the PC, the \mathbf{R}_{ij} matrices can be computed by adding one layer at a time [2-4] with recursive relations given by

$$\begin{aligned}\mathbf{R}_{11}(z) &= \mathbf{R}_{11}(z - \Delta z) \\ &+ \mathbf{R}_{12}(z - \Delta z)(\mathbf{r}_{11}(\Delta z) - \mathbf{R}_{22}(z - \Delta z))^{-1} \mathbf{R}_{21}(z - \Delta z)\end{aligned}\quad (14)$$

$$\mathbf{R}_{12}(z) = -\mathbf{R}_{12}(z - \Delta z)(\mathbf{r}_{11}(\Delta z) - \mathbf{R}_{22}(z - \Delta z))^{-1} \mathbf{r}_{21}(\Delta z) \quad (15)$$

$$\mathbf{R}_{21}(z) = \mathbf{r}_{21}(\Delta z)(\mathbf{r}_{11}(\Delta z) - \mathbf{R}_{22}(z - \Delta z))^{-1} \mathbf{R}_{21}(z - \Delta z) \quad (16)$$

$$\mathbf{R}_{22}(z) = \mathbf{r}_{22}(\Delta z) - \mathbf{r}_{21}(\Delta z)(\mathbf{r}_{11}(\Delta z) - \mathbf{R}_{22}(z - \Delta z))^{-1} \mathbf{r}_{21}(\Delta z) \quad (17)$$

To start the recursion with the initial layer, the starting point in Eqs. (14)-(17) is evident when $z = 0$ in Eq. (10) and $L = \Delta z$ in Eq. (13) or $\mathbf{R}_{ij}(\Delta z) = \mathbf{r}_{ij}(\Delta z)$, where Δz is the thickness of the initial layer. All layers can be of different thickness and repeated application of Eqs. (14)-(17) yields the matrix relationship given in Eq. (13) for $L = L_z$. With this we have related the fields across the PC up to, but not including, the source layer. The last layer, which includes the antenna, is discussed below.

R-Matrix with sources

To include a source within the last antenna layer of thickness h we modify the R-matrix relationship analogous to Eq. (10) as

$$\begin{pmatrix} E(L_z) \\ E(L_z + h) \end{pmatrix} = \begin{pmatrix} \mathbf{r}_{11}(h) & \mathbf{r}_{12}(h) \\ \mathbf{r}_{21}(h) & \mathbf{r}_{22}(h) \end{pmatrix} \begin{pmatrix} B(L_z) \\ B(L_z + h) \end{pmatrix} + \frac{4\pi i \omega}{c^2} \begin{pmatrix} \mathbf{M}_a^{-1} J \\ \mathbf{M}_a^{-1} J \end{pmatrix} \quad (18)$$

where the subscript a on \mathbf{M}_a refers to the antenna layer. We next use Eqs. (13) and (18) to find

$$\begin{aligned} \begin{pmatrix} E(0) \\ E(L_z + h) \end{pmatrix} &= \begin{pmatrix} \mathbf{R}_{11}(L_z + h) & \mathbf{R}_{12}(L_z + h) \\ \mathbf{R}_{21}(L_z + h) & \mathbf{R}_{22}(L_z + h) \end{pmatrix} \begin{pmatrix} B(0) \\ B(L_z + h) \end{pmatrix} \\ &+ \frac{4\pi i \omega}{c^2} \begin{pmatrix} -\mathbf{R}_{12}(L_z)(\mathbf{r}_{11}(h) - \mathbf{R}_{22}(L_z))^{-1} \mathbf{M}_a^{-1} J \\ (\mathbf{I} - \mathbf{r}_{21}(h)(\mathbf{r}_{11}(h) - \mathbf{R}_{22}(L_z))^{-1}) \mathbf{M}_a^{-1} J \end{pmatrix}. \end{aligned} \quad (19)$$

Note that this equation explicitly contains \mathbf{R} matrices evaluated at two different arguments. The $L_z + h$ argument in the \mathbf{R} matrices includes the PC structure *and* source layer. Likewise, the L_z argument includes only the PC structure. The \mathbf{r}_{ij} matrices pertain only to the source layer. In order to solve this equation for the surface fields $E(0)$, $E(L_z + h)$, $B(0)$, and $B(L_z + h)$, we need a relationship between the electric and magnetic fields.

Transmitted and reflected radiation field

We apply continuity conditions that the tangential field components of the electric and magnetic fields are continuous across the $z=0$ and $z=L_z+h$ interfaces. This allows coupling with the fields in the semi-infinite homogeneous superstrate $z \geq L_z+h$ and substrate $z \leq 0$. If we denote the superstrate and substrate by $+$ and $-$ superscripts, respectively, then the continuity conditions can be written as

$$E^-(0) = E(0) \quad , \quad B^-(0) = B(0) \quad , \quad (20)$$

$$E^+(L_z+h) = E(L_z+h) \quad , \quad \text{and} \quad B^+(L_z+h) = B(L_z+h) \quad . \quad (21)$$

Since the superstrate and substrate are homogeneous, the electric and magnetic fields can easily be related, and we use such relationships in Eq. (19). This allows E^\pm and B^\pm to be calculated. The power radiated away from the surface is proportional to $P^\pm = \Re \int dx E^\pm(x,z) [B^\pm(x,z)]^*$ and from this we calculate the non-normalized distribution of radiated power to be

$$\frac{dP^\pm}{d\mathbf{q}} = \frac{w/c}{2p} \cos \mathbf{q} \Re \left[E^\pm(k) (B^\pm(k))^* \right] \quad (22)$$

where $k = (w/c) \sin \mathbf{q}$ and \mathbf{q} is the polar angle of radiation measured from the z direction. Note that the E and B fields have been Fourier transformed into k -space since we are interested in the angular distribution of radiation.

Numerical Results

For numerical analysis, we consider the PC shown in Fig. 1. All material media are assumed to be non-dispersive for all frequencies with the permittivity of the dielectric rods $\mathbf{e}_a = (9,0)$, the background medium $\mathbf{e}_b = (1,0)$, and the wire antenna $\mathbf{e}_w = (-100,30)$. The superstrate and substrate regions above and below the PC have permittivity $(1, 0)$. The side dimension of the square rods is given by the fill factor of 0.156 or $w = 0.395a$. In Fig. 1, the PC consists of 37 periods in the x direction or $L_x = 37a$ and 6 whole periods in the z direction or $L_z = 6a$. The dimensions of the rectangular antenna are width $0.5a$ and height $0.2a$.

In the numerical results, the number of digitization points for the x dimension is $N = 701$ which yields a spatial resolution of $\Delta x = 37a/N = 0.053a$. The PML region on each side of the PC consists of 30 layers for a total thickness of $30\Delta x$. Within these layers, $\mathbf{s}_x(x) = \mathbf{e}(x)\mathbf{s}_x^*(x)$, and the conductivity is quadratically increased with depth into the PML layers region.

Calculated antenna radiation

In Fig. 2, the k - ω dispersion curves are shown for TE polarized electromagnetic wave propagation in an *infinite* photonic crystal. The design parameters for the infinite PC are the same as described for the finite-sized PC in Fig. 1. In other words, the x and z dimensions of the PC for the dispersion data shown in Fig. 2 are unbounded. Figure 2 also shows that there is a band gap that approximately spans $w/c = 0.32(2p/a) \rightarrow 0.43(2p/a)$. The PC in Fig. 1 is not infinite, but is nevertheless large enough so that the information in Fig. 2 can be applied to the truncated PC. In Figs. 3, 4 and 5, we show the calculated antenna radiation at frequencies below, within, and above the band gap edges. The frequencies marked by the arrows on the left side of Fig. 2 are $w/c = 0.2(2p/a)$, $0.38(2p/a)$, and $0.5(2p/a)$. If $w/c = 2p/l$, where λ is the free space wavelength for angular frequency ω , then we see that these three w/c values yield $l = 5a$, $l = 2.63a$, and $l = 2a$, respectively. In Fig. 3, it is seen that there is radiation in both transmission and reflection. This is to be expected since the frequency is below the band gap. In Fig. 4, the frequency is within the band gap and there is no transmitted radiation. This is consistent with the existence of an energy band gap at this frequency. For comparison, the dotted line shows the result for antenna radiation when a thick metal film having the same permittivity as the wire antenna replaces the PC. The complex permittivity of the antenna is assumed to be $(-100, 30)$. This radiated intensity is slightly less than that for the PC presumably because of absorption by the metal. Finally, Fig. 5 shows the radiation pattern for a frequency above the band gap. Here there is again some transmitted radiation as well as much more reflected radiation at larger angles when compared to Fig. 4.

Parallelization Results

The computer code used to obtain numerical results involved eigenvalue-eigenvector computation, matrix-matrix and matrix-vector multiplication, and linear equation system solution. In the serial code, the bulk of computational effort was spent on eigenvalue-eigenvector computation and this prompted the effort to develop a complex asymmetric eigensolver routine. This work resulted in the development of two new computational routines: pzlahqr and pztrvc.

The eigenvalues of a Hessenberg matrix \mathbf{A} are obtained by computing the Schur factorization $\mathbf{T} = \mathbf{Q}^H \mathbf{A} \mathbf{Q}$, where \mathbf{T} is upper triangular and the eigenvalues of \mathbf{A} are the diagonal entries of \mathbf{T} . The eigenvectors can be computed by backward substitution. The complex asymmetric eigensolver was modeled on the ScaLAPACK [5] code pdlahqr, which is designed to compute eigenvalues of a real non-symmetric matrix in parallel. In keeping with ScaLAPACK notation, the new code, which computes eigenvalues of a complex non-symmetric matrix in parallel, is named pzlahqr. The output from pzlahqr is used to then calculate the eigenvectors in pztrvc (based on the serial ztrvc). For the code used in this work, it is required that process grids be chosen in square blocks of 1×1 , 2×2 , 3×3 , etc. However, in general, pzlahqr and pztrvc can use any size rectangular grid.

The performance of pzlahqr is shown in Figs. 6, 7, and 8. All performance runs were done on the Origin 2000 at ERDC MSRC. Figure 6 shows time in seconds versus size of problem N for serial and 1×1 to 4×4 process grid. Significant wallclock reduction is evident but

the advantage gained when going beyond a 2×2 process grid rapidly diminishes. In Fig. 7, the speedup relative to a 1×1 process grid, versus size of problem, is shown. Finally, in Fig. 8, the megaflops versus size of problem is shown for serial and several process grids.

Conclusions

We have presented theory and numerical results for radiation of a long antenna that is flush mounted atop a finite-sized photonic crystal substrate. We have also developed complex non-symmetric eigensolver codes based on ScaLAPACK [5] methodology.

The numerical results for antenna radiation indicate that for a frequency within the band gap, the radiation pattern is very similar to that for a metallic substrate. While this indicates that use of a PC would emulate the radiation characteristics of a metal substrate, the big advantage would be preventing potential heat damage. It has been estimated that heat absorption for a PC relative to a Cu metal substrate would be about two orders of magnitude less.[6]

Parallelization performance results have also been presented for the eigensolver routine. A speedup of about 3 is seen for a 2×2 process grid relative to a 1×1 process grid. Going to a 4×4 process grid yields a relative speedup of about 4. Prior to the UGC2000 Conference, only a minimal amount of benchmark testing has been accomplished. At this point the rapidly diminishing speedup gains are likely due to a small problem size and much more extensive testing is forthcoming. In any case, since the bulk of the computational time was originally spent with serial LAPACK complex asymmetric eigensolver routines, the development of the complex parallel eigensolver routines promises to yield much decreased wallclock times.

Acknowledgments

The use of computing resources at the NAVO and ERDC MSRC facilities and their support personnel is gratefully acknowledged.

References

- [1] Jean-Pierre Berenger, "A perfectly matched layer for the absorption of electromagnetic waves," J. Comp. Phys. 114, pp. 185-200 (1994); Jean-Pierre Berenger, "Three-dimensional perfectly matched layer for the absorption of electromagnetic waves," J. Comp. Phys. **127**, pp. 363-379 (1996).
- [2] J. M. Elson, and P. Tran, "Dispersion and diffraction in photonic media: A different modal expansion for the **R**-matrix propagation technique," J. Opt. Soc. Am. A **12**, 1765-1771 (1995).
- [3] J. M. Elson, and P. Tran, "Coupled mode calculation with the **R**-matrix propagator for the dispersion of surface waves on a truncated photonic crystal," Phys. Rev. B **54**, 1711-1715 (1996).
- [4] J. M. Elson, and P. Tran, "Band structure and transmission of photonic media: a real-space finite-difference calculation with the **R**-matrix propagator," in *Photonic Band Gap Materials*, Vol. 315, *NATO Advanced Study Institute Series E: Applied Sciences*, edited by C. M. Soukoulis (Kluwer, Dordrecht, 1996), pp. 341-354
- [5] "ScaLAPACK Users' Guide", L. S. Blackford, J. Choi, A. Cleary, E. D'Azevedo, J. Demmel, I. Dhillon, J. Dongarra, S. Hammarling, G. Henry, A. Petitet, K. Stanley, D. Walker, and R. C. Whaley, published by SIAM, Philadelphia, PA, (1997).
- [6] E. R. Brown, O. B. McMahon, C. D. Parker, C. Dill III, K. Agi, and K. J. Malloy, "Microwave applications of photonic crystals", in *Photonic Band Gap Materials*, Vol. 315, *NATO Advanced Study Institute Series E: Applied Sciences*, edited by C. M. Soukoulis (Kluwer, Dordrecht, 1996), pp. 355-375

Figure Captions

Figure 1. Schematic showing modeling of photonic crystal (PC) and antenna. The crystal period is a in both the x and z directions. The dark shaded squares are the dielectric rods of side width w and the antenna is the black rectangle, of thickness h , in the topmost layer. For numerical analysis, the PC has total x length $L_x = 37a$ and z length $L_z = 6a$. The fill factor is $w^2/a^2 = 0.189$ and the material parameters for the rods (dark gray) and background (light gray) are $\mathbf{e}_r = (9, 0)$ and $\mathbf{e}_b = (1, 0)$. The two vertical shaded areas at the x limits of the PC are absorption layers. Any two adjacent horizontal dashed lines indicate layers that are by definition z invariant with respect to material parameters.

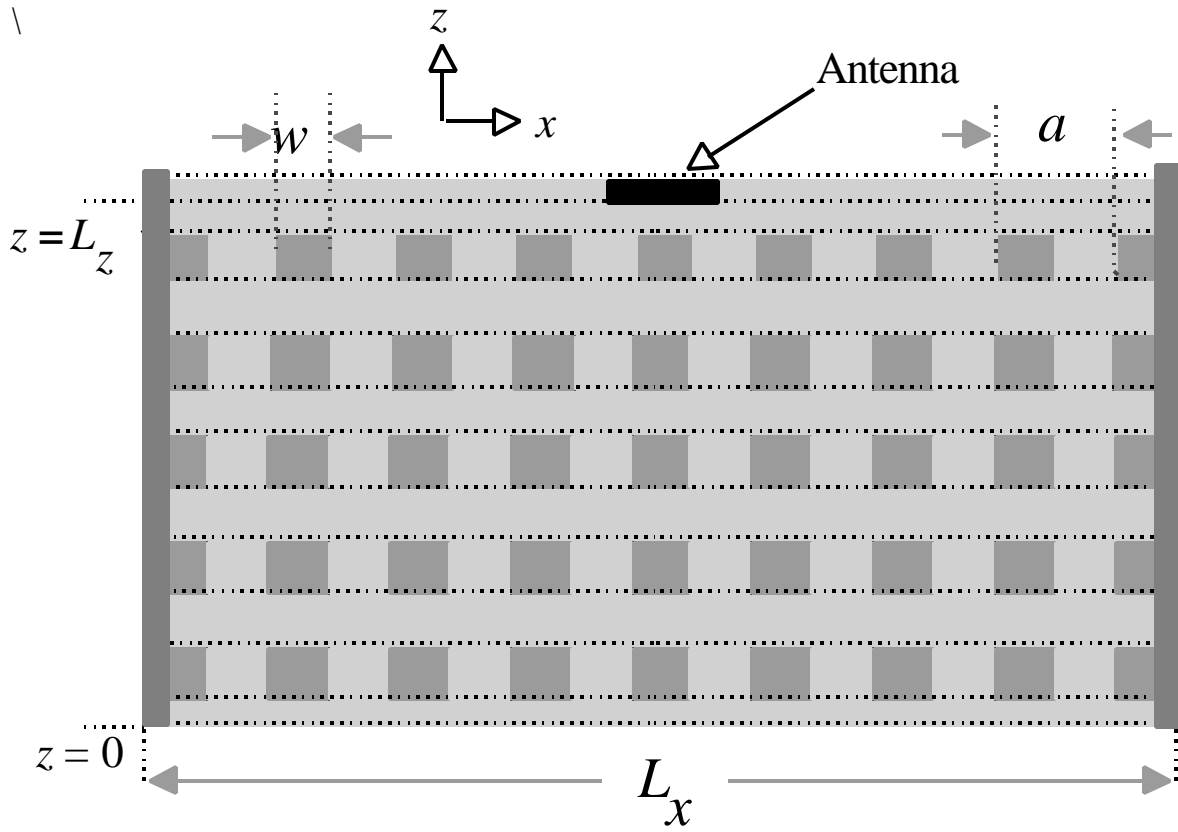


FIG. 1 (ELSON-FAHEY)

Figure 2. Band structure diagram for a two-dimensionally infinite PC with the electric field polarized parallel to the rods. The horizontal shaded area indicates a complete band gap. The three arrows indicate frequencies below, within, and above the band gap which are used in the numerical analysis.

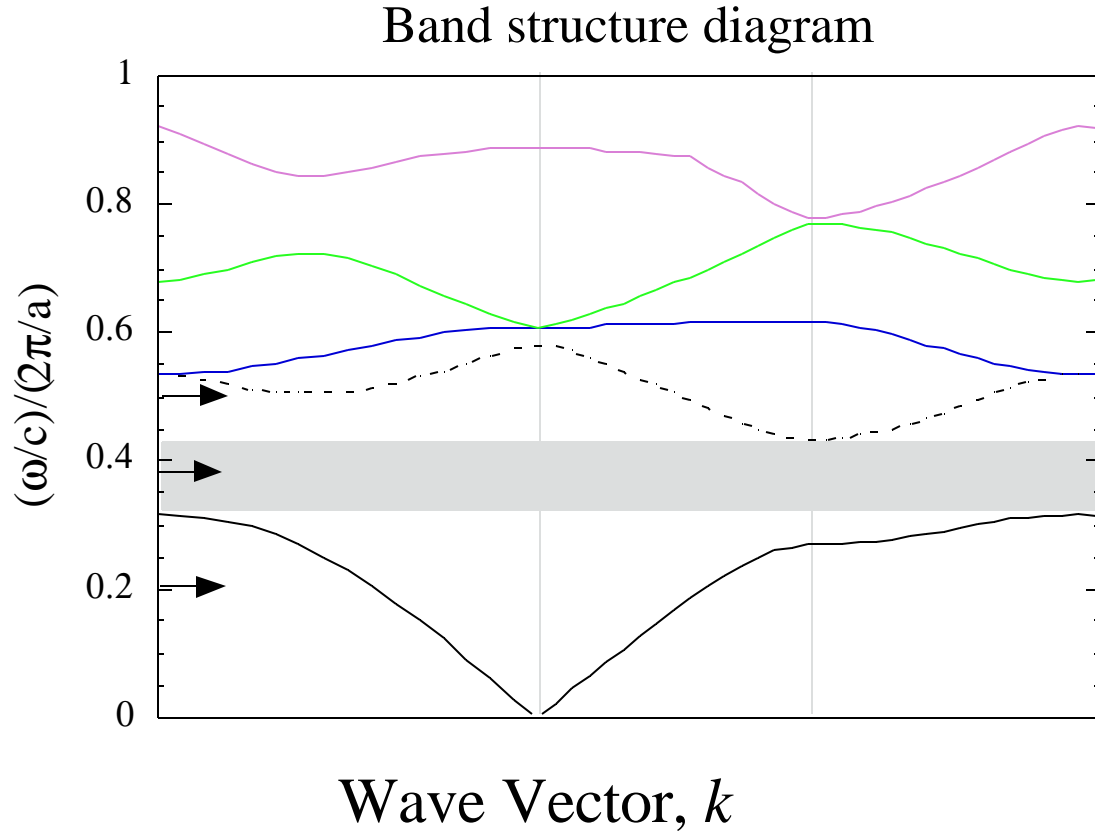


FIG. 2 (ELSON-FAHEY)

Figure 3. Polar plot of radiation pattern versus radiation angle into the superstrate and substrate for $(w/c) = 0.2(2p/a)$. At this frequency, which is below the band gap, there is radiation into the substrate.

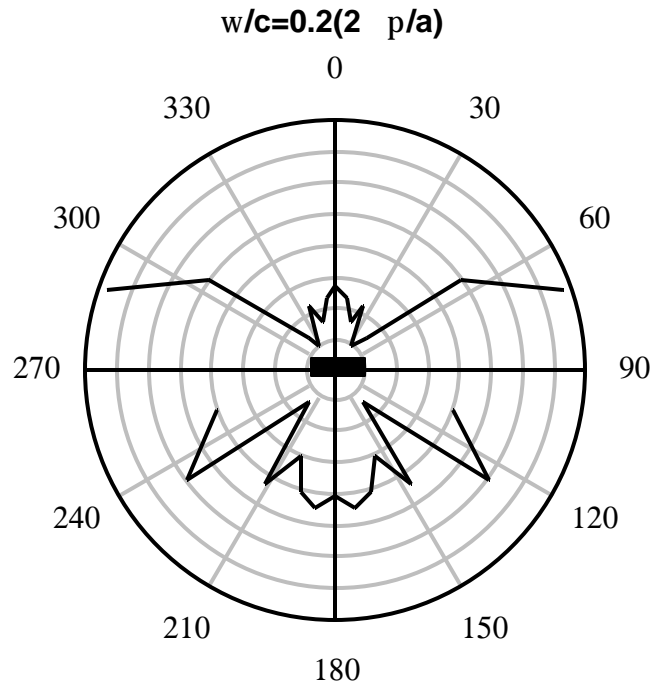


FIG. 3 (ELSON, FAHEY)

Figure 4. Polar plot (solid curve) of radiation pattern versus radiation angle into the superstrate for $(w/c) = 0.38(2p/a)$. Since this frequency is within the band gap, there is no radiation into the substrate. For comparison, the dotted curve shows the corresponding calculation when the PC region $z \leq L_z$ is replaced by a metal with permittivity the same as that for the antenna.

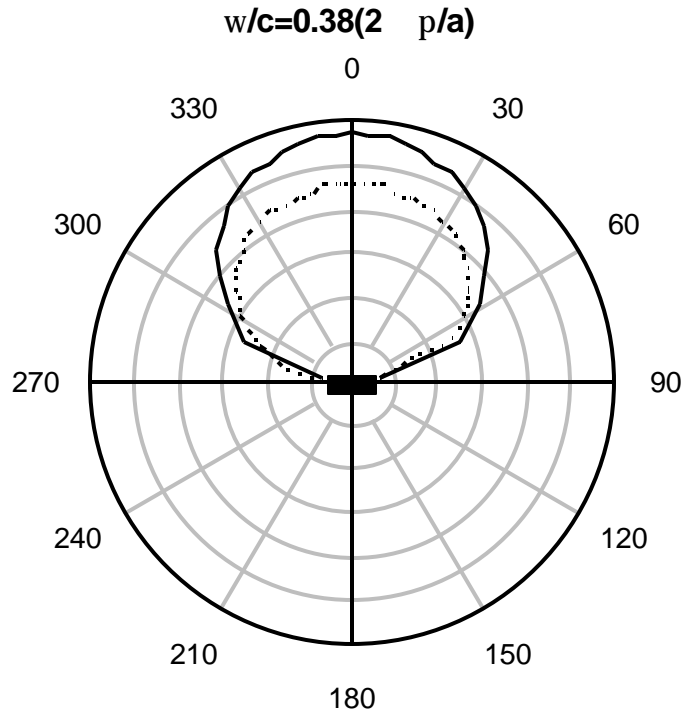


FIG. 4 (ELSON, FAHEY)

Figure 5. Polar plot of radiation pattern versus radiation angle into the superstrate and substrate for $(w/c) = 0.50(2p/a)$. At this frequency, which is above the band gap, there is some radiation into the substrate.

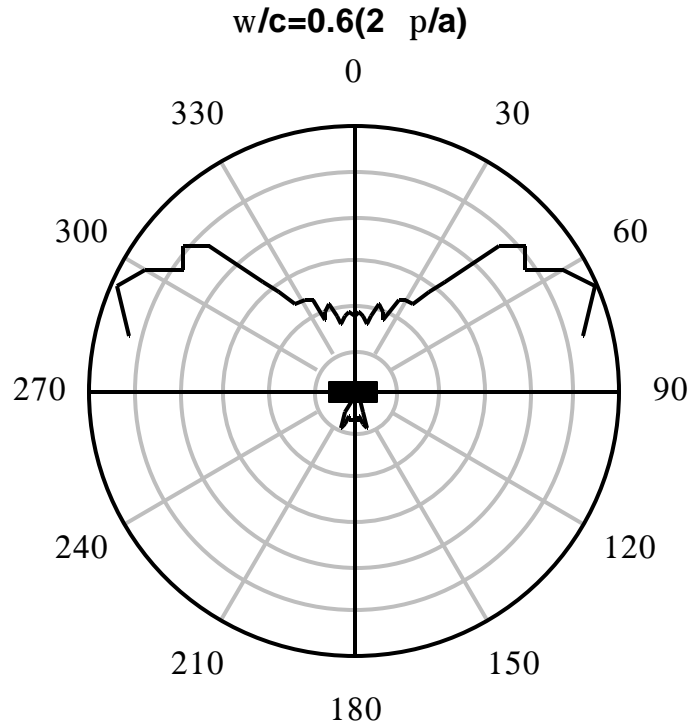


FIG. 5 (ELSON, FAHEY)

Figure 6. Eigensolver performance: time in seconds versus size of problem N . The serial curve (diamond) is compared with several square process grids.

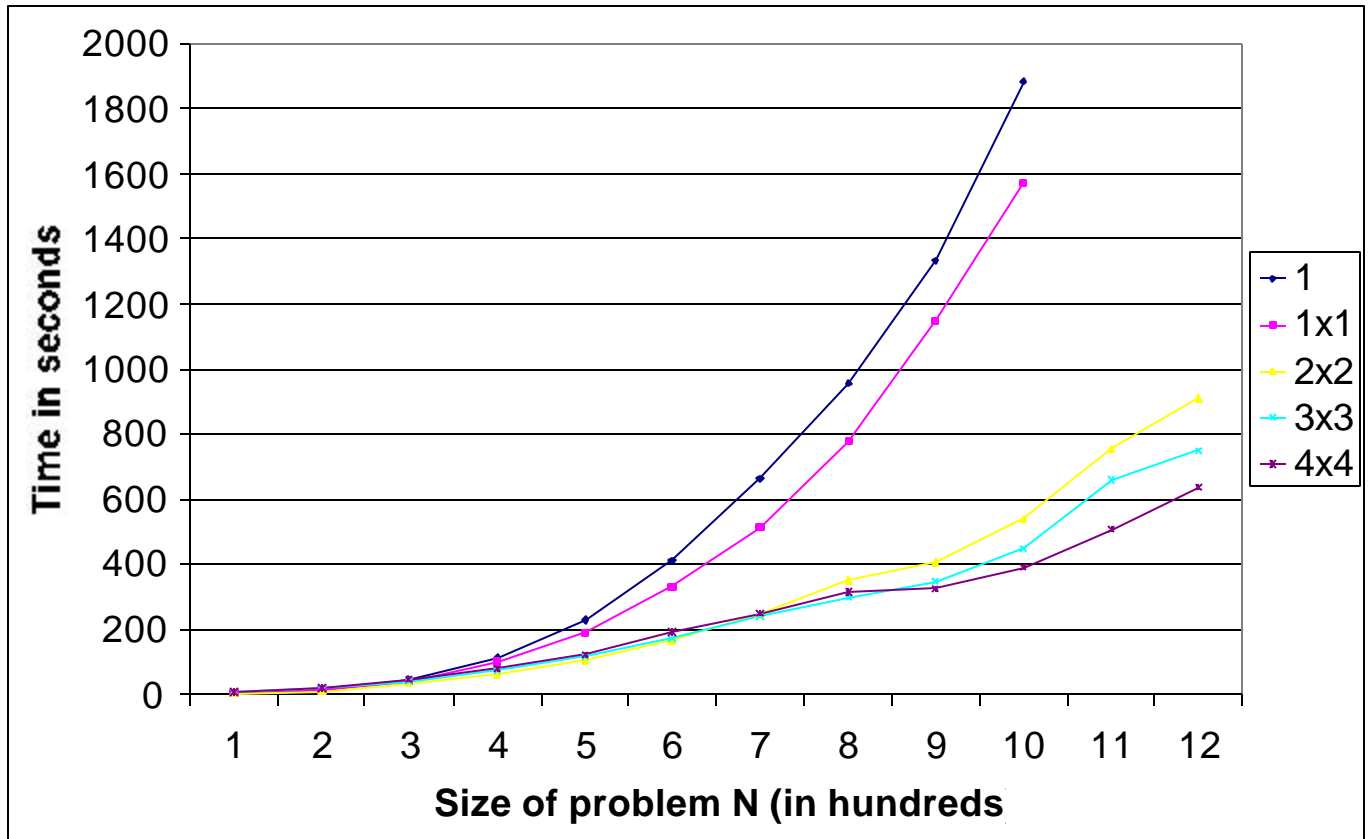


FIG. 6 (ELSON, FAHEY)

Figure 7. Eigensolver performance: speedup relative to 1×1 process grid versus size of problem N . The serial curve (diamond) is slightly slower than the reference 1×1 process grid. The larger process grids exhibit a relative speedup from 3-4 times.

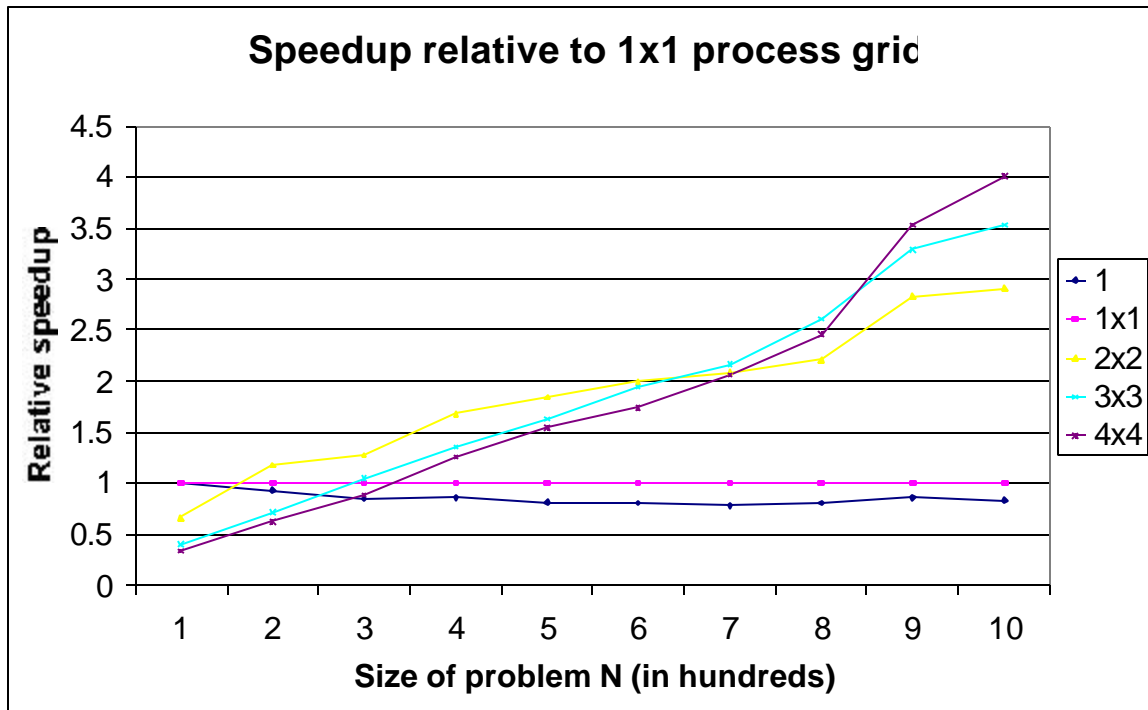


FIG. 7 (ELSON, FAHEY)

Figure 8. Eigensolver performance: megaflops versus size of problem N . The serial curve (diamond) is compared with several square process grids.

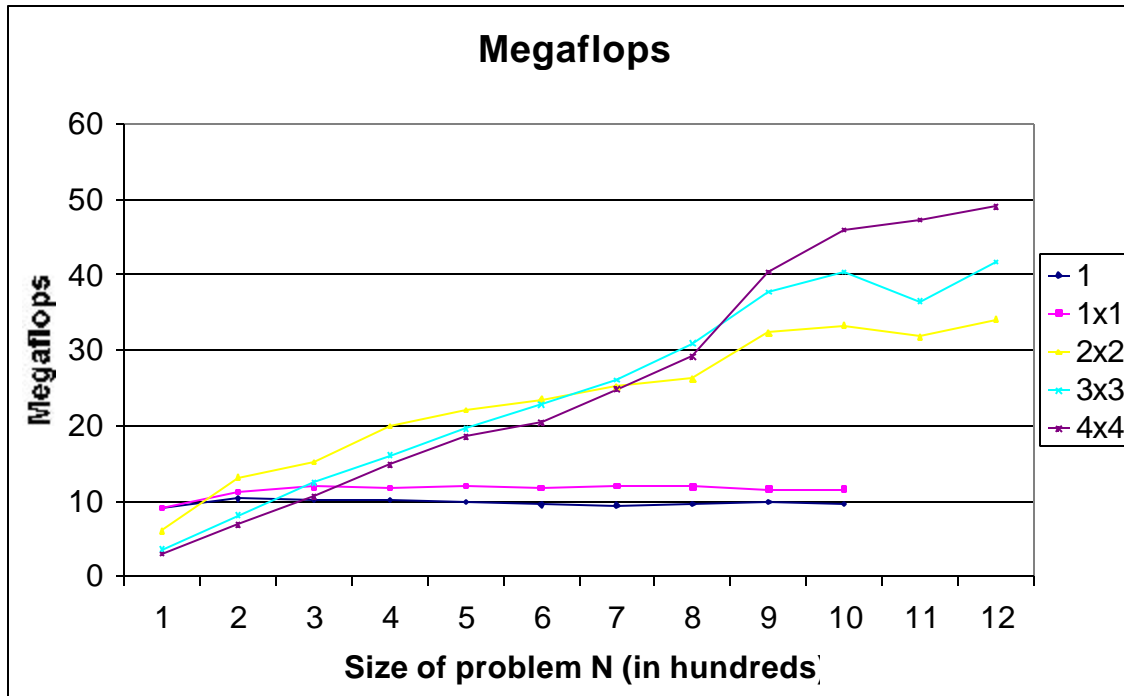


FIG. 8 (ELSON, FAHEY)